Engineering Fracture Mechanics 288 (2023) 109293

Contents lists available at ScienceDirect

Engineering Fracture Mechanics

journal homepage: www.elsevier.com/locate/engfracmech

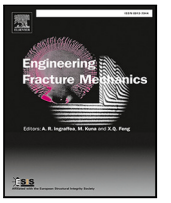

Crack tip solution for Mode III cracks in spring interfaces

Sara Jiménez-Alfaro [a,b], Vladislav Mantič [b,*]

[a] Institut Jean Le Rond d'Alembert, Sorbonne Université, Pl. Jussieu, 4, Paris, 75005, France
[b] Grupo de Elasticidad y Resistencia de Materiales, Escuela Técnica Superior de Ingenieria, Universidad de Sevilla, Camino de los Descubrimientos, Sevilla, 41092, Spain

ARTICLE INFO

Keywords:
Antiplane strain
Adhesive interface
Interface fracture
Asymptotic solution
Logarithmic stress singularity

ABSTRACT

Considering an infinite linear elastic isotropic solid in antiplane shear, the Mode III crack-tip solution for a semi-infinite crack located in a straight spring interface is systematically studied for the first time. A new analytic expression for this crack-tip solution is given in the form of a double asymptotic series of the main and the so-called associated shadow terms. It is shown that the series of the shadow terms associated with a main term is infinite, and all shadow terms include logarithmic terms. Thus, although the interface tractions are bounded, the linear elastic solution at this crack-tip has a logarithmic stress singularity which is comprehensively analysed. Noteworthy, the character of this stress singularity is very different from the well-known square root singularity at the crack tip in the classical fracture mechanics. A key advantage of the present approach is its simplicity, as only elementary mathematical tools are employed, and also its easy implementation in a computer algebra software. The latter fact is very relevant because the expressions of higher-order shadow terms become increasingly complicated, so their generation by a computer code becomes crucial. The present results allow the implementation of new enriched or singular crack-tip finite elements for such cracks, and the automatic generation of analytic solutions for benchmark problems for testing the finite-element codes using these special elements. Such codes can be applied to efficient numerical modelling of interface cracks, e.g., in adhesively bonded joints with a thin adhesive layer.

1. Introduction

The classical Winkler spring interface model [1], which considers a continuous distribution of independent linear elastic springs, is widely used to solve many engineering problems due to simplicity of analytical studies and for the sake of computational efficiency in numerical models. In particular, thin adhesive layers are often modelled using the related shear-lag model [2] and its generalizations [3,4]. A recent review of the spring model can be found in [5], and comprehensive classifications of interface models including the spring model in [6,7].

Design and analysis of adhesively bonded joints working under different loading conditions requires suitable computational models for crack onset and propagation in adhesive layers [8]. In this context, although several models on different scales exist for the study of crack initiation and growth in adhesive layers, one of the most widely used in analytical and computational studies is the spring interface, also referred to as weak, imperfect, linear elastic or Robin interface, see [9–14].

It is well known that according to a general mathematical analysis of singularities in elliptic partial differential equations developed in [15,16], the displacements and stresses around a singular point can be described analytically through an asymptotic series expansion, including power-logarithmic terms in the radial variable.

* Corresponding author.
E-mail address: mantic@us.es (V. Mantič).

https://doi.org/10.1016/j.engfracmech.2023.109293
Received 13 January 2023; Received in revised form 18 April 2023; Accepted 22 April 2023
Available online 4 May 2023

Nomenclature

$a_{j,k}^{(l)}, b_{j,k}^{(l)}$	Constant coefficients in the asymptotic series
$\mathbf{B}_{j,k}$	Vector of coefficients in the system of equations
e_j	Relative error in the Robin boundary condition
k	Stiffness of the linear-elastic spring distribution
K_j	Generalized Stress Intensity Factors (GSIFs)
μ	Shear modulus
G	Energy Release Rate (ERR)
$\mathbf{G}_{j,k}$	Right-hand side vector of the system of equations
$\mathbf{M}_{j,k}$	Matrix of the system of equations
L	Characteristic length in the studied problem
N	Number of main terms considered in the asymptotic series
S_j	Number of shadow terms considered for the jth main term
u^e, u^o	Even and odd part of the out-of-plane displacement solution
u_j	jth element of the asymptotic series
u_j^k	kth shadow term associated to the jth main term
x, y	Cartesian coordinates
δ	Virtual crack length increment
γ	Governing parameter of the problem
Γ_1, Γ_2	Boundary parts
λ_j	Singularity exponent
Ω^+, Ω^-	Upper and lower half domain
r, θ	Polar coordinates
σ_{rz}, $\sigma_{\theta z}$	Stress components in the cylindrical coordinates system
BVP	Boundary Value Problem
ERR	Energy Release Rate
FEM	Finite Element Method
GSIF	Generalized Stress Intensity Factor
LEFM	Linear Elastic Fracture Mechanics
N–N	Neumann–Neumann problem
N–R	Neumann–Robin problem
R–N	Robin–Neumann problem

Considering a particular case of a crack in a thin adhesive layer modelled by a spring interface, the question about the character of the asymptotic crack-tip solution arises, which seems to be quite different from that of a crack in a homogeneous linear elastic material described by the classical Linear Elastic Fracture Mechanics (LEFM). As it can be seen in the asymptotic series for the crack tip solution in LEFM, deduced in [17,18] for plane problems (Mode I and II), and in [19] for antiplane shear problems (Mode III), stresses near the crack tip have singular solutions, with square root singularities, multiplied by Stress Intensity Factors (SIFs). In particular, the asymptotic series for the Mode III crack-tip solution can be easily obtained by separation of variables applied to the displacement solution in polar coordinates, as shown, e.g., in [20].

The behaviour of stresses and displacements around the tip of a crack situated in a spring interface has not been fully characterized so far, although some relevant results have been obtained by several authors [10–13,21–25], indicating that a logarithmic stress singularity takes place at such a crack-tip. Especially significant for the present work are the contributions [22,23], for the antiplane elastic problem, and [24], for the plane elastic problem, who deduced the first terms of the asymptotic expansions at the tip of a crack situated at a spring type interface. While an approach based on the well-known Wieghardt–Williams procedure was used in [22], more advanced mathematical tools such as singular integral equations and Mellin transformations were used in [23,24].

Regarding the related asymptotic series for corners (angular sectors) of any interior angle with spring type boundary condition, several relevant results were obtained by various authors. Truncated asymptotic series including also logarithmic terms were introduced in [22,26–28] to approximate the linear elastic solutions in corners of various specific angles with spring boundary condition at one or both faces, for antiplane and plane elasticity. However, the number of terms in these asymptotic series was quite limited. A general mathematical approach for the Laplace equation in corners with one or two spring (Robin) boundary conditions, based on the solution of suitably defined recursive boundary value problems (BVPs), was introduced in [29]. These developments motivated a more computationally oriented procedure presented in [30], for the singularity analysis of linear elastic corners under antiplane shear with a spring boundary condition on one corner face.

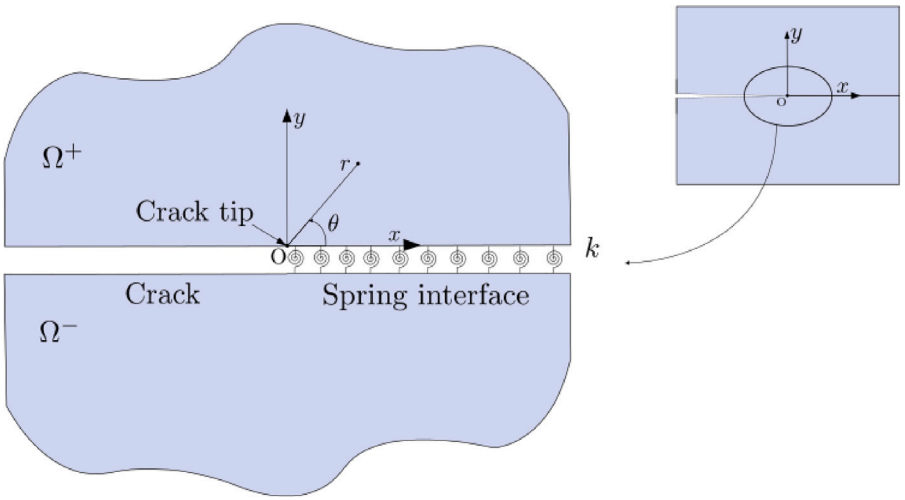

Fig. 1. A semi-infinite crack in a straight spring (adhesive) interface between two half-planes. Notice that the spring distribution is acting in the out-of-plane direction.

In the present paper, the antiplane solution for a semi-infinite crack located in a straight spring-interface between two linear elastic isotropic half-planes of the same material is deduced in the form of an asymptotic series, for the first time. This series represents the local solution in the neighbourhood of the tip of a finite crack in a linear elastic (spring type) interface. Due to symmetry arguments the solution is decomposed into a symmetric and a skew-symmetric part with respect to the interface line. Whereas the symmetric part of this solution is given by a series of smooth functions, the skew-symmetric part is given by the singular Mode III solution. An analytic expression for the displacements in this Mode III solution is given in the form of a double asymptotic series of the main and the so-called associated shadow terms. It is shown that the series of the shadow terms associated to a main term is infinite and all shadow terms include logarithmic terms. Therefore, the solution for stresses at the crack tip includes a logarithmic stress singularity, this singularity being comprehensively analysed. This Mode III solution, can be considered as the crack-tip solution in Mode III for a crack in a locally straight spring-interface between linear elastic adherents of the same isotropic material.

A key advantage of the present novel procedure is its simplicity and the fact that it provides the complete asymptotic series for the crack-tip solution, which is an advantage in comparison to some previous related works where only the first terms were presented. Moreover, it can be easily implemented in a computer algebra software, like Mathematica [31], which has been shown to be a key feature as the higher-order shadow terms become progressively increasingly complicated. The automatic generation of the expressions for the terms of the asymptotic series can be very useful for their usage in the implementation of new enriched or singular crack-tip finite elements for cracks propagating in spring interfaces, and also for the generation of testing problems for FEM codes.

In Section 2 the antiplane shear problem for a semi-infinite crack at a straight spring-interface is formulated, and the symmetry arguments are used to reduce it to a corner-singularity problem for a half-plane. Then, in Section 3 the analytic procedure based on the complex variable formulation is presented, a pseudocode implementing this procedure being shown in Section 4. The analytical expressions for the main terms and for the first two shadow terms are presented in Section 5. Graphical representations of the singular solution, given by a number of terms in the asymptotic series providing a sufficiently high accuracy of plots, are shown and discussed in Section 6. Finally, the Energy Release Rate (ERR) is computed for a crack in a spring interface by the Irwin crack closure integral in Section 7.

2. Description of the model

As mentioned in Section 1, the aim of this paper is to study an antiplane elastic problem of a semi-infinite crack in a straight spring interface between two half-planes (two half-spaces in 3D view) of the same linear elastic isotropic materials. Therefore, linear elastic springs are acting in the out-of-plane z-direction. The solution of the problem is described in terms of the out-of-plane displacement $u(x,y) = u_z(x,y)$, a harmonic function that can be approximated by an asymptotic series expansion in the vicinity of the crack-tip. The crack-tip is located at the origin O of the Cartesian coordinate system, see Fig. 1.

The considered BVP (P^{c}), defined in the two-half planes, $(\Omega^+ \cup \Omega^-) \subset \mathbb{R}^2$, bonded by a semi-infinite spring interface, represented in Fig. 1, is formulated as follows

$$\Delta u = 0 \qquad \text{in } \Omega^+ \cup \Omega^-, \tag{1}$$

$$(\mathrm{P}^{\mathrm{c}}) \qquad \sigma_{yz} = k\left[u(x,0^+) - u(x,0^-)\right] \qquad \text{for } x > 0 \text{ and } y = 0, \tag{2}$$

$$\sigma_{yz} = 0 \qquad \text{for } x < 0 \text{ and } y = 0. \tag{3}$$

Along the positive part of the x-axis the adhesive interface between half-planes Ω^+ and Ω^- is modelled by a continuous distribution of linear elastic springs, known in the applied-mathematics community as the Robin boundary condition, cf. [29,32], which is characterized by the stiffness $k = k_z > 0$, associated to the out-of-plane z-direction. The semi-infinite crack located along the negative part of the x-axis is described by the stress-free condition.

The stress component $\sigma_{yz}(x, y)$ is related to $u(x, y)$ using the constitutive law $\sigma_{yz} = \mu\, u_{,y}$ and $\sigma_{xz} = \mu\, u_{,x}$, with $\mu > 0$ being the shear elastic modulus of the bulk material. Therefore, (2) and (3) can be rewritten as

$$\frac{\partial u}{\partial y} = \frac{k}{\mu}\left[u(x, 0^+) - u(x, 0^-)\right] \qquad \text{if } x > 0 \text{ and } y = 0, \tag{4}$$

$$\frac{\partial u}{\partial y} = 0 \qquad \text{if } x < 0 \text{ and } y = 0. \tag{5}$$

Similarly as in [33], the solution $u(x, y)$ is decomposed as the sum of an even (symmetric) and an odd (skew-symmetric) part with respect to the coordinate y, as

$$u^{\mathrm{e}}(x, y) = \frac{u(x, y) + u(x, -y)}{2} = u^{\mathrm{e}}(x, -y), \tag{6}$$

$$u^{\mathrm{o}}(x, y) = \frac{u(x, y) - u(x, -y)}{2} = -u^{\mathrm{o}}(x, -y). \tag{7}$$

The superscripts $^{\mathrm{e}}$ and $^{\mathrm{o}}$ denote the even and the odd part, respectively, the sum of them gives the original-problem solution,

$$u(x, y) = u^{\mathrm{e}}(x, y) + u^{\mathrm{o}}(x, y). \tag{8}$$

As we can see from (6) and (7), once we know u^{e} or u^{o} in a half plane, Ω^+ or Ω^-, it is also given in the other half-plane.

Applying the definitions for $u^{\mathrm{e}}(x, y)$ and $u^{\mathrm{o}}(x, y)$, and the equilibrium of tractions on the interface (i.e., the continuity of σ_{yz} and of $u_{,y}$ across the interface), the BVP (P^{c}) previously presented is split into two problems defined, e.g., in the half-plane Ω^+. The first one is for the even part of $u(x, y)$

(P^{e})

$$\Delta u^{\mathrm{e}} = 0 \qquad \text{in } \Omega^+, \tag{9}$$

$$\frac{\partial u^{\mathrm{e}}}{\partial y} = 0 \qquad \text{if } x > 0 \text{ and } y = 0, \tag{10}$$

$$\frac{\partial u^{\mathrm{e}}}{\partial y} = 0 \qquad \text{if } x < 0 \text{ and } y = 0, \tag{11}$$

and the second for the odd part of $u(x, y)$

(P^{o})

$$\Delta u^{\mathrm{o}} = 0 \qquad \text{in } \Omega^+, \tag{12}$$

$$\frac{\partial u^{\mathrm{o}}}{\partial y} = \gamma u^{\mathrm{o}}(x, 0^+) \qquad \text{if } x > 0 \text{ and } y = 0, \tag{13}$$

$$\frac{\partial u^{\mathrm{o}}}{\partial y} = 0 \qquad \text{if } x < 0 \text{ and } y = 0. \tag{14}$$

A governing parameter γ of dimension 1/length used in (13) is defined as

$$\gamma = \frac{2k}{\mu}. \tag{15}$$

The solutions to the BVP (P^{e}) in the Cartesian coordinates system are given by any finite linear combination or an infinite series of a subset of homogeneous harmonic polynomials, which include an even power of y, as it was obtained in [33]. These homogeneous harmonic polynomials can be written in the polar coordinates system as

$$u_j^e(r, \theta) = r^{\lambda_j} \cos(\lambda_j \theta), \qquad \text{for } \lambda_j = j - 1, \qquad j \in \mathbb{N}. \tag{16}$$

For example, for $j = 1$, 2 and 3, these polynomial solutions to the BVP (P^{e}) written in Cartesian coordinates are: $u_j^e(x, y) = 1$, x and $x^2 - y^2$. Notice that in (16) the index $j \in \mathbb{N}$[1] to avoid an infinite energy in the vicinity of the crack-tip, which corresponds to the case $j \leq 0$ and $j \in \mathbb{Z}$.

The BVP named as (P^{o}) is solved and studied in the following sections. This problem is also called the Robin–Neumann problem because of the boundary conditions imposed on the boundary of the half-plane Ω^+, the x-axis. For the sake of notation simplicity, in the next sections the odd part of the complete problem solution, which corresponds to a spring interface with a crack under Mode III loading condition, will be also denoted as $u = u^{\mathrm{o}}$. Noteworthy, the solution u^e and u^o are not unique, because no remote boundary conditions are prescribed at infinity.

[1] The following subsets of real numbers will be used in this work: $\mathbb{Z}$ the set of integer numbers, $\mathbb{N}$ the set of natural numbers.

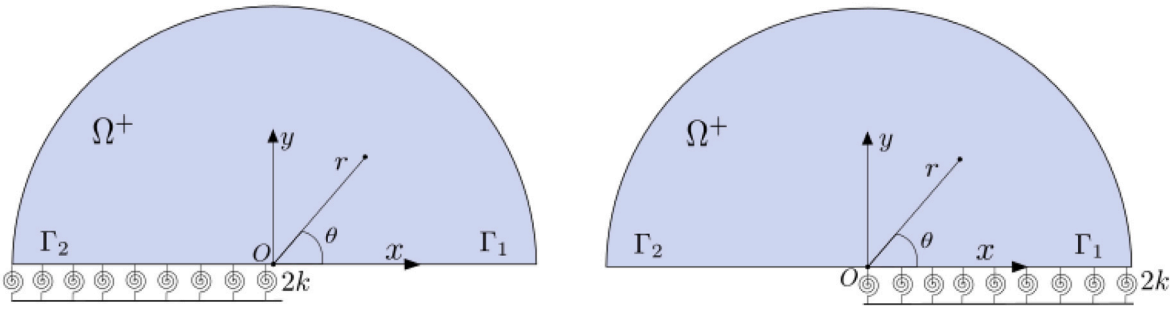

(a) Neumann-Robin (b) Robin-Neumann

Fig. 2. Scheme of the problem in the vicinity of the singularity. Notice that the spring distribution is acting in the out-of-plane direction.

3. Deduction of the asymptotic series expansion

The solution to the Robin–Neumann problem (P^o) in Ω^+ can be represented by a doubly infinite asymptotic series expansion, which can be considered as a particular case of the general asymptotic expansion deduced in [30] for corners, by setting the inner angle of corner (angular sector) as $\omega = \pi$, i.e. defining a half-plane. The jth element of this series, denoted as u_j, is defined by the sum of a main term (main singularity) $u_j^{(0)}$ and an infinite series of shadow terms (shadow singularities) $u_j^{(k)}$. This doubly infinite asymptotic series expansion can be approximated by a truncated series of N terms u_j, each one with S_j shadow terms,

$$u(r,\theta) \approx \sum_{j=1}^{N} K_j u_j(r,\theta) = \sum_{j=1}^{N} K_j \left(u_j^{(0)}(r,\theta) + \sum_{k=1}^{S_j} u_j^{(k)}(r,\theta) \right), \tag{17}$$

For N and S_j going to infinity the complete doubly infinite asymptotic series is recovered. The coefficients K_j are called *Generalized Stress Intensity Factors* (GSIFs), and are defined by the overall configuration of the problem, i.e., the loads applied and the whole geometry of the specimen. The expression (17) is written in a polar coordinates system that is located at the origin O, the crack tip, as it can be seen in Fig. 2.

For the sake of simplicity in the application of the boundary conditions, first we find the asymptotic series expansions of the solution for the so-called Neumann–Robin (N–R) problem, see Fig. 2(a). Then, by a change of variable

$$\theta = \pi - \theta, \tag{18}$$

the solution to the Robin–Neumann (R–N) problem is obtained, see Fig. 2(b). This change is made to follow the tradition of representing a crack growing from left to right, so in Fig. 2(b), Γ_2 corresponds to the upper face of the crack.

The main terms $u_j^{(0)}$ are calculated replacing the Robin boundary condition (13) by a homogeneous Neumann boundary condition, i.e., solving the Neumann–Neumann problem. Its analytical solution is given by an asymptotic series whose terms are in fact defined in (16). As follows from (16) and (17), the dimension of K_j is $(\text{length})^{1-\lambda_j} = (\text{length})^{2-j}$. It is important to highlight that only $j \in \mathbb{N}$ are considered, since an infinite strain energy is obtained for $j \leq 0$, as explained above.

The shadow terms $u_j^{(k)}$ in the N–R problem, with $k = 1, \ldots, S_j$, are obtained by solving the following recursive BVPs

$$(P_j^k) \qquad \begin{aligned} \Delta u_j^{(k)} &= 0 \qquad \text{in } \Omega^+, && (19)\\ \frac{\partial u_j^{(k)}}{\partial \theta} &= 0 \qquad \text{on } \Gamma_1, && (20)\\ \frac{1}{r}\frac{\partial u_j^{(k)}}{\partial \theta} &= -\gamma u_j^{(k-1)} \qquad \text{on } \Gamma_2, && (21) \end{aligned}$$

where Γ_1 and Γ_2 are the boundary parts defined by $y = 0$ and $x > 0$ and $x < 0$, respectively, see Fig. 2(a).

Following [30], terms $u_j^{(k)}(r,\theta)$ are given by the complex variable expression written as

$$u_j^{(k)}(z) = \sum_{l=0}^{k} \left[a_{j,k}^{(l)} \cdot \text{Im}\left\{ z^{\lambda_j + k} \log^l z \right\} + b_{j,k}^{(l)} \cdot \text{Re}\left\{ z^{\lambda_j + k} \log^l z \right\} \right], \tag{22}$$

where the complex number associated to a point in the upper half-plane is $z = x + iy = r\exp(i\theta)$, and $a_{j,k}^{(l)}$ and $b_{j,k}^{(l)}$ are real constant coefficients providing real valued displacements $u_j^{(k)}(z)$. Since k is the index related to each shadow term in the series, we can observe that the maximum power of the logarithmic terms in the expression of u_j is increased each time we include an additional shadow term in the series. The expression in (22) can be rewritten using real variables and applying the binomial expansion as

$$u_j^{(k)}(r,\theta) = r^{\lambda_j + k} \sum_{l=0}^{k} \sum_{m=0}^{l} \binom{l}{m} \log^m(r)\, \theta^{l-m} \left[a_{j,k}^{(l)} \sin t_{j,k}^{(l-m)}(\theta) + b_{j,k}^{(l)} \cos t_{j,k}^{(l-m)}(\theta) \right], \tag{23}$$

where $\binom{l}{m} = \frac{l!}{m!(l-m)!}$ and

$$t_{j,k}^{(l-m)}(\theta) = (\lambda_j + k)\theta + \frac{\pi(l-m)}{2}. \tag{24}$$

Regarding the homogeneous Neumann boundary condition in (20), we have

$$\left.\frac{\partial u_j^{(k)}}{\partial \theta}\right|_{\theta=0} = r^{(\lambda_j+k)} \sum_{l=0}^{k} a_{j,k}^{(l)} \left((\lambda_j + k)\log^l r + l\log^{l-1} r\right) = 0. \tag{25}$$

In order to fulfil (25) for all $r > 0$, coefficients $a_{j,k}^{(l)}$ for all j, k and l are zero. The Robin boundary condition in (21) is written using real variables and simplifying terms r^{λ_j+k-1} in both sides as

$$\begin{aligned}&\sum_{l=0}^{k} b_{j,k}^{(l)} \sum_{m=0}^{l} \binom{l}{m} \log^m(r)\pi^{l-m}\left[\frac{l-m}{\pi}\cos t_{j,k}^{(l-m)}(\pi) - (\lambda_j + k)\sin t_{j,k}^{(l-m)}(\pi)\right] \\ &= -\gamma \sum_{l=0}^{k-1} b_{j,k-1}^{(l)} \sum_{m=0}^{l} \binom{l}{m} \log^m(r)\pi^{l-m}\cos t_{j,k-1}^{(l-m)}(\pi).\end{aligned} \tag{26}$$

Since (26) must be verified for all $r > 0$, coefficients $b_{j,k}^{(l)}$ are determined by comparing terms with the same power of $\log^m r$ on both sides of the equation, leading to a linear system of $k+1$ equations. For each kth shadow term, this system is expressed in matrix form as

$$\mathbf{M}_{j,k}\mathbf{B}_{j,k} = \mathbf{G}_{j,k}, \tag{27}$$

to determine the vector of coefficients $\mathbf{B}_{j,k} = \left[b_{j,k}^{(0)}, \ldots, b_{j,k}^{(m)}, \ldots, b_{j,k}^{(k)}\right]^T$. The terms in the vector $\mathbf{G}_{j,k} = \left[G_{j,k}^{(0)}, \ldots, G^{(m)}, \ldots, G_{j,k}^{(k)}\right]^T$ are written, after some simplifications, as

$$G_{j,k}^{(m)} = \gamma \sum_{l=m}^{k-1} b_{j,k-1}^{(l)} \binom{l}{m} \pi^{l-m}\cos\left[\frac{\pi(l-m)}{2}\right], \text{for } 0 \le m < k, \tag{28}$$

$$G_{j,k}^{(k)} = 0. \tag{29}$$

This last element of the vector $\mathbf{G}_{j,k}$ is always zero because it is associated with the kth power of the logarithm, and in the $(k-1)$th shadow term (the shadow term used to define the vector $\mathbf{G}_{j,k}$) this power does not appear.

The overall structure of the square matrix $\mathbf{M}_{j,k}$ is

$$\mathbf{M}_{j,k} = \begin{bmatrix} 0 & \cdots & M_{j,k}^{(0,l)} & \cdots & M_{j,k}^{(0,k)} \\ 0 & \ddots & & & \vdots \\ \vdots & \ddots & \ddots & & \vdots \\ \vdots & & 0 & \ddots & \vdots \\ 0 & \cdots & \cdots & 0 & 0 \end{bmatrix}, \tag{30}$$

where each term of the matrix is expressed, after some simplifications, as

$$M_{j,k}^{(m,l)} = \binom{l}{m}\pi^{l-m}\left[\frac{l-m}{\pi}\cos\left[\frac{\pi(l-m)}{2}\right] - (\lambda_j + k)\sin\left[\frac{\pi(l-m)}{2}\right]\right] \qquad \text{for } m < l, \tag{31}$$

$$M_{j,k}^{(m,l)} = 0 \qquad \text{for } m \ge l. \tag{32}$$

Since the first column of the matrix $\mathbf{M}_{j,k}$ is zero, the first coefficient $b_{j,k}^{(0)}$ is undefined, and the terms $u_j^{(k)}(r,\theta)$ are not unique. However, it can be verified that the singularity order related to the coefficient $b_{j,k}^{(0)}$, $\lambda_j + k$, is equal to the singularity order of other main term in the series, $j' > j$, which is $\lambda_{j'} = \lambda_j + k$. The difference between two particular solutions of Eqs. (19)–(21) is therefore the solution to the Neumann–Neumann problem, which means that it is included in the main term in the other j'th element of the series, as it was explained for a general case in [30]. Thus, for the sake of simplicity and without lost of generality we can assume

$$b_{j,k}^{(0)} = 0, \qquad \text{for } k \ge 1. \tag{33}$$

Hence, the non-uniqueness of the solution would be solved if we considered an infinite series for the solution, which is, unfortunately, numerically impossible. On the other hand, coefficients $b_{j,k}^{(m)}$ for $m \ne 0$ are expressed taking advantage of the fact that the matrix $\mathbf{M}_{j,1}$ has upper triangular form, and therefore they can be obtained by a procedure similar to the Gaussian back substitution,

$$b_{j,k}^{(k)} = \frac{G_{j,k}^{(k-1)}}{M_{j,k}^{(k-1,k)}}, \tag{34}$$

$$b_{j,k}^{(l)} = \frac{1}{M_{j,k}^{(l-1,l)}}\left[G_{j,k}^{(l-1)} - \sum_{s=l+1}^{k} M_{j,k}^{(l-1,s)} b_{j,k}^{(s)}\right], \text{ for } 1 \le l \le k-1. \tag{35}$$

Notice that the initial vector of coefficients, for $k = 1$, is defined through the main term, $u_j^{(0)}(r,\theta)$. This is equivalent to set $b_{j,0}^{(0)} = 1$ in the iterative process we have described.

Moreover, remember that in this section we have obtained the solution to the Neumann–Robin (N–R) problem in Ω^+. Therefore, the change of variable given in (18) is applied to (23) to get the shadow terms in the so-called Robin–Neumann (R–N) problem. As it has been shown in this section, solving N–R has less computational complexity than solving R–N, because coefficients $a_{j,k}^{(l)}$ are reduced to zero by applying the Neumann boundary condition at $\theta = 0$.

Finally, with a finite number of terms in the asymptotic series the Robin boundary condition is not exactly fulfilled. Nevertheless, the error decreases in the vicinity of the crack tip when more shadow terms are included in the series, i.e., S_j is increased. Therefore, a suitable choice of S_j depends on the desired accuracy of the solution, which can be defined through the relative error $e_j(r)$,

$$e_j(r) = \frac{\frac{1}{r}\frac{\partial u_j}{\partial \theta}(r,0)}{\gamma u_j(r,0)} - 1 \overset{?}{\approx} 0. \tag{36}$$

The minimum number of shadow terms S_j to be included in the truncated series depends on the range of r where an accuracy, defined by a maximum value of error, is requested. A study of the function $e(r)$ in this range is required to decide a suitable value of S_j. Notice that higher S_j lead to higher computational complexities.

The order (in terms of the power of r) of the error of a truncated series increases with increasing S_j. This leads to more accurate approximations of the exact solution in a vicinity of the crack tip by the series with increasing S_j, but outside this region the higher-order terms diverge more rapidly than the lower order terms, so the truncated series with a higher S_j can provide worse approximations for the solution far away from the crack tip, see e.g. Fig. 9. Recall that a similar behaviour can be observed in approximations of smooth functions by the Taylor series.

4. Pseudocode computing asymptotic series expansion

A key advantage of the above procedure to deduce the asymptotic series expansion for a semi-infinite crack in a straight spring interface is that its implementation in computer algebra software is straightforward and very efficient. Thus, this implementation allows to obtain a fully analytical solution in terms of truncated series, which depends on how many shadow terms are considered in the series associated to a jth main term. In the following lines we propose a pseudocode implementing this procedure for R–N problem. In this code, $B[k,l]$ represents the unknown coefficients.

Define γ, G, j, S_j

$$\lambda_j = j - 1,\ u_j^{(0)}(r,\theta) = r^{\lambda_j}\cos\lambda_j\theta,\ \text{and}\ B[0,0] = 1$$

$$t[\theta,k,l,m] = (\lambda_j + k)\theta + \frac{\pi(l-m)}{2}$$

For $k = 1$ **To** S_j **Do**

$$M[m,l] = \binom{l}{m}\pi^{(l-m)}\left[\frac{l-m}{\pi}\cos\left[\frac{\pi(l-m)}{2}\right] - (\lambda_j + k)\sin\left[\frac{\pi(l-m)}{2}\right]\right]$$

$$G[m] = \gamma\sum_{l=m}^{k-1} B[k-1,l]\binom{l}{m}\pi^{l-m}\cos\left[\frac{\pi(l-m)}{2}\right]$$

$$B[k,k] = \frac{G[k-1]}{M[k-1,k]}\ \text{and}\ B[k,0] = 0$$

For $l = k - 1$ **To** 1 **Do**

$$B[k,l] = \frac{1}{M[l-1,l]}\left[G[l-1] - \sum_{s=l+1}^{k} M[l-1,s]B[k,s]\right]$$

EndFor

EndFor

$$u_j(r,\theta) = u_j^{(0)}(r,\theta) + \sum_{k=1}^{S_j} r^{\lambda_j+k}\sum_{l=0}^{k} B[k,l]\sum_{m=0}^{l}\binom{l}{m}\log^m(r)\theta^{l-m}\cos(t[\theta,k,l,m])$$

$$u_j(r,\theta) = u_j(r,\pi-\theta)$$

$$e_j(r) = \frac{\frac{1}{r}\frac{\partial u_j}{\partial\theta}(r,0)}{\gamma u_j(r,0)} - 1$$

$$\sigma_{rzj}(r,\theta) = \mu \frac{\partial u_j(r,\theta)}{\partial r}$$

$$\sigma_{\theta zj}(r,\theta) = \frac{\mu}{r} \frac{\partial u_j(r,\theta)}{\partial \theta}$$

5. Explicit expressions of the first two terms of the asymptotic series solution

In this section, we deduce explicit expressions of the first terms of the asymptotic series solution for a semi-infinite crack situated in a straight spring interface, following the theoretical procedure explained above. We first solve the Neumann–Robin and then the Robin–Neumann problem shown in Fig. 2, deducing the expressions of the first two shadow terms, i.e., $S_j = 2$, for the sake of simplicity, giving

$$u_j(r,\theta) = u_j^{(0)}(r,\theta) + u_j^{(1)}(r,\theta) + u_j^{(2)}(r,\theta), \tag{37}$$

where the main term representing a solution to the homogeneous Neumann–Neumann problem for the upper half-plane is expressed as

$$u_j^{(0)}(r,\theta) = r^{j-1}\cos[(j-1)\theta], \tag{38}$$

see (16) and the associated discussion.

5.1. Explicit expressions for the Neumann–Robin problem

For a better understanding of the matrix procedure explained above for the Neumann–Robin problem, see (27), the coefficients $b_{j,k}^{(l)}$ in (22), are explicitly computed for $k = 1$ and 2. As it was previously mentioned, the recursive explicit expressions for $b_{j,k}^{(l)}$ can be obtained by a procedure similar to the Gaussian back substitution (34)–(35), which also has lower computational complexity.

For the first shadow term, $k = 1$, the following system of equations $\mathbf{M}_{j,1}\mathbf{B}_{j,1} = \mathbf{G}_{j,1}$ is solved, applying (28)–(29) to compute vector $\mathbf{G}_{j,1}$ and (31)–(32) to compute matrix $\mathbf{M}_{j,1}$. The resulting system has the form

$$\begin{pmatrix} 0 & -j\pi \\ 0 & 0 \end{pmatrix} \begin{pmatrix} b_{j,1}^{(0)} \\ b_{j,1}^{(1)} \end{pmatrix} = \begin{pmatrix} \gamma \\ 0 \end{pmatrix}. \tag{39}$$

This gives $b_{j,1}^{(1)} = \frac{-\gamma}{j\pi}$ and $b_{j,1}^{(0)} = 0$, see (33). By substituting these coefficients in (23), the final expression of the first shadow term, $k = 1$, for the N–R problem, is obtained,

$$u_j^{(1)}(r,\theta) = \frac{\gamma r^j}{j\pi}\left[\theta\sin(j\theta) - \log r\cos(j\theta)\right]. \tag{40}$$

Similarly, the system of equations for the second shadow term, $k = 2$, is obtained,

$$\begin{pmatrix} 0 & -\pi(1+j) & -2\pi \\ 0 & 0 & -2\pi(1+j) \\ 0 & 0 & 0 \end{pmatrix} \begin{pmatrix} b_{j,2}^{(0)} \\ b_{j,2}^{(1)} \\ b_{j,2}^{(2)} \end{pmatrix} = \begin{pmatrix} 0 \\ -\frac{\gamma^2}{j\pi} \\ 0 \end{pmatrix}. \tag{41}$$

The solution of this system gives the expressions for the coefficients $b_{j,2}^{(0)} = 0$, $b_{j,2}^{(1)} = \frac{-\gamma^2}{j\pi^2(1+j)^2}$ and $b_{j,2}^{(2)} = \frac{\gamma^2}{2\pi^2 j(1+j)}$, see (33). The final expression for the second shadow term, $k = 2$, is

$$u_j^{(2)}(r,\theta) = \frac{-\gamma^2 r^{1+j}}{j(j+1)\pi^2}\left[U_1(r,\theta) + U_2(r,\theta)\right], \tag{42}$$

where

$$U_1(r,\theta) = \frac{-1}{(j+1)}\left(\theta\sin[(1+j)\theta] - \cos[(1+j)\theta]\log r\right) \tag{43}$$

$$U_2(r,\theta) = \frac{1}{2}\left[\cos[(1+j)\theta]\theta^2 + \log r\; 2\theta\sin[(1+j)\theta] - \log^2 r\cos[(1+j)\theta]\right]. \tag{44}$$

By combining the previous expressions (38), (40) and (42), the asymptotic series solution of the N–R problem in (37) for $j = 1$ with two shadow terms, $S_1 = 2$, is obtained

$$u_1(r,\theta) = 1 + \frac{\gamma r}{\pi}\left[\theta\sin(\theta) - \cos(\theta)\log r\right] + \frac{r^2\gamma^2}{4\pi^2}\left\{-\theta^2\cos 2\theta + \theta\sin 2\theta - (\cos 2\theta + 2\theta\sin 2\theta)\log r + \cos 2\theta\log^2 r\right\}. \tag{45}$$

Noteworthy, the main term $u_1^{(0)}$ is given by a unit rigid body translation in the $z-$direction. The stress components associated with this solution are

$$\sigma_{\theta z1}(r,\theta) = \frac{\gamma\mu}{\pi}\left[\theta\cos\theta + \sin\theta + \sin\theta\log r\right] + \frac{r\mu\gamma^2}{4\pi^2}\left[\sin 2\theta(1+2\theta^2) - 4\theta\cos 2\theta\log r - 2\sin 2\theta\log^2 r\right], \tag{46}$$

$$\sigma_{rz1}(r,\theta) = \frac{\gamma\mu}{\pi}\left[\theta\sin\theta - \cos\theta - \cos\theta\log r\right] - \frac{r\mu\gamma^2}{4\pi^2}\left[\cos 2\theta(1+2\theta^2) + 4\theta\sin 2\theta\log r - 2\cos 2\theta\log^2 r\right], \tag{47}$$

As follows from expressions (46) and (47), both stress components have a logarithmic singularity at the singular point $r = 0$. Nevertheless, as it could be expected, $\sigma_{\theta z1}$ is bounded along the negative part of the x-axis ($\theta = \pi$) in the neighbourhood of this singular point, due to the Robin boundary condition there, whereas it vanishes along the positive part of the x-axis ($\theta = 0$).

It should be mentioned that Sinclair [22] presented the singular solution for the displacement $u_1(r,\theta)$ up to the first shadow term and for the stress $\sigma_{\theta z1}(r,\theta)$ up to the second shadow term, matching the corresponding parts of the expressions (45) and (46), respectively.

5.2. Explicit expressions for the Robin–Neumann problem

As explained in Section 3, the asymptotic series solution of the R–N problem in (37) with two shadow terms, $S_1 = 2$, can be easily obtained by applying the change of variable (18) to the asymptotic series solution of the N–R problem in (45),

$$\begin{aligned} u_1(r,\theta) &= 1 + \frac{\gamma r}{\pi}\left[(\pi-\theta)\sin\theta + \cos\theta\log r\right] \\ &\quad + \frac{\gamma^2 r^2}{4\pi^2}\left[-(\pi-\theta)\sin 2\theta - (\pi-\theta)^2\cos 2\theta - (-2(\pi-\theta)\sin 2\theta + \cos 2\theta)\log r + \cos 2\theta\log^2 r\right]. \end{aligned} \tag{48}$$

The stresses corresponding to these displacements are expressed as

$$\begin{aligned} \sigma_{\theta z1}(r,\theta) &= -\frac{\gamma\mu}{\pi}\left[\sin\theta - (\pi-\theta)\cos\theta + \sin\theta\log r\right] \\ &\quad + \frac{r\mu\gamma^2}{4\pi^2}\left[(2(\pi-\theta)^2+1)\sin 2\theta + 4(\pi-\theta)\cos 2\theta\log r - 2\sin 2\theta\log^2 r\right], \end{aligned} \tag{49}$$

and

$$\begin{aligned} \sigma_{rz1}(r,\theta) &= \frac{\gamma\mu}{\pi}\left[(\pi-\theta)\sin\theta + \cos\theta + \cos\theta\log r\right] \\ &\quad + \frac{r\mu\gamma^2}{4\pi^2}\left[-\left(1+2(\pi-\theta)^2\right)\cos 2\theta + 4(\pi-\theta)\sin 2\theta\log r + 2\cos 2\theta\log^2 r\right]. \end{aligned} \tag{50}$$

Similarly as in the N–R problem, these stresses have a logarithmic singularity at $r = 0$, and $\sigma_{\theta z1}$ is bounded along the positive part of the x-axis ($\theta = 0$) near the singular point.

Remark. According to Mishuris [23], displacements and stresses in the upper half domain of this R–N problem are expressed as

$$u_M \approx \frac{1}{\pi\mu}\left\{\frac{\mu_*\tau_*\pi}{1+\mu_*}a_0^- + [G_M(-1) - c_0^- - a_0^-(1-\log r)]r\cos\theta + a_0^-(\pi-\theta)r\sin\theta\right\}, \tag{51}$$

$$\sigma_{\theta zM} \approx -\frac{1}{\pi}\left[a_0^-\log r\sin\theta + [G_M(-1) - c_0^-]\sin\theta - a_0^-(\pi-\theta)\cos\theta\right], \tag{52}$$

$$\sigma_{rzM} \approx \frac{1}{\pi}\left[a_0^-\log r\cos\theta + [G_M(-1) - c_0^-]\cos\theta + a_0^-(\pi-\theta)\sin\theta\right], \tag{53}$$

where the original author's notation, with a subscript "M" indicating a solution or parameter by Mishuris [23], is employed. In the present case, the materials, in the upper and in the lower half-planes, are considered identical. For this reason, $\mu_* = 1$. Moreover, the function $G_M(s) = \mu\frac{\partial u}{\partial\theta}(s,\pi)$ evaluated in $s = -1$ is $G_M(-1) = 0$. The coefficient $\tau_* = \frac{2}{\gamma}$. Therefore, we get

$$u_M \approx \frac{a_0^-}{\gamma\mu} - \frac{(c_0^- + a_0^-)}{\pi\mu}r\cos\theta + \frac{ra_0^-}{\pi\mu}\cos\theta\log r + \frac{ra_0^-}{\pi\mu}(\pi-\theta)\sin\theta, \tag{54}$$

$$\sigma_{\theta zM} \approx \frac{-1}{\pi}\left[a_0^-\sin\theta\log r - c_0^-\sin\theta - a_0^-(\pi-\theta)\cos\theta\right], \tag{55}$$

$$\sigma_{rzM} \approx \frac{1}{\pi}\left[a_0^-\cos\theta\log r - c_0^-\cos\theta + a_0^-(\pi-\theta)\sin\theta\right], \tag{56}$$

which can be compared to our solution for $j = 1$ and $S_1 = 1$,

$$u_1(r,\theta) = 1 + \frac{r\gamma}{\pi}\cos\theta\log r + \frac{r\gamma}{\pi}(\pi-\theta)\sin\theta, \tag{57}$$

$$\sigma_{\theta z1}(r,\theta) = -\frac{\gamma\mu}{\pi}\left[\sin\theta\log r + \sin\theta - (\pi-\theta)\cos\theta\right] \tag{58}$$

$$\sigma_{rz1}(r,\theta) = \frac{\gamma\mu}{\pi}\left[\cos\theta\log r + \cos\theta + (\pi-\theta)\sin\theta\right]. \tag{59}$$

If we normalize Mishuri's solution in (54) by considering $a_0^- = \gamma\mu$, we get the same solution as in (57) except of a term given by a constant times $r\cos\theta$, which represents the following higher order main term for $j = 2$ in (38). It is easy to see that this difference is associated with the choice of $b_{j,k}^{(0)} = 0$ in (33). Actually, taking $a_0^- = \gamma\mu$ and $c_0^- = -\gamma\mu$, the solution obtained in [23] in (54)–(56) is exactly the same as the one deduced in the present paper given by expressions (57)–(58), for $j = 1$ and $S_1 = 1$.

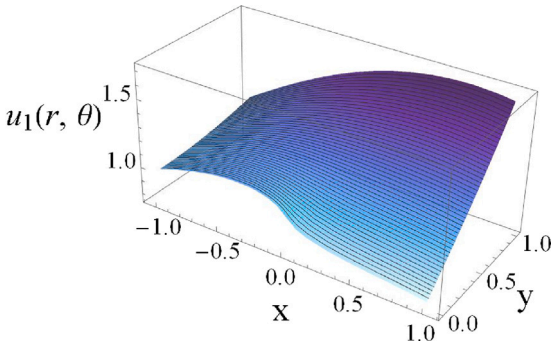

Fig. 3. Out-of-plane displacement $u_1(r,\theta)$ in a rectangular plate, for $\gamma = 1$ and $S_1 = 8$.

Note that the solution in [23] essentially corresponds to the first main term $j = 1$ and the first shadow term $S_1 = 1$, whereas the present work allows us to easily compute an asymptotic series expansion for any number of main terms and up to any order of the shadow terms. In fact, in the next section, asymptotic solutions with shadow terms up to order of $S_1 = 8$ are used to achieve a high accuracy of the solutions plotted. Furthermore, in the supplementary material, shadow terms up to forth order, $S_1 = 4$, are included for the sake of completeness. As it will be shown in the following section, the error in the Robin boundary condition is reduced in the vicinity of the crack-tip when more shadow terms are used to approximate the solution.

6. Graphical representation of the solution for the Robin–Neumann problem

In this section the first term $u_1(r,\theta)$ of the series (17), solving the R–N problem, is represented, since it is the one related to stress singularities in the vicinity of the crack-tip. The total number of shadow terms employed is indicated in each figure, and the maximum number of shadow terms used is $S_1 = 8$ or 9. The main reason for this selection is the error in the Robin boundary condition in the neighbourhood of the crack-tip, discussed at the end of the section, with the aim to achieve a sufficiently high accuracy of the plots of solutions presented. Recall that we are representing here just the skew-symmetric part of the full-crack-problem solution, which is the non-smooth and singular one, denoted in Section 2 as $u^o(r,\theta)$. The singular part of the crack solution can be completed by any smooth even part of the crack solution $u^e(r,\theta)$. For the sake of simplicity, in the graphical representations we consider the shear modulus $\mu = 1$ in this section.

In Fig. 3 the out-of-plane displacement $u_1(r,\theta)$ in the upper half-plane Ω^+ is represented in a rectangle $[-1,1]\times[0,1]$, for $\gamma = 1$. Notice that the solution in the lower half-plane Ω^- is skew-symmetric with respect to the x-axis, i.e., $u(x,-y) = -u(x,y)$. It is observed that the displacement is higher at the upper crack face at $\theta = \pi$ (homogeneous Neumann boundary condition) than at the upper face of the springs interface at $\theta = 0$ (Robin boundary condition).

The evolution of the out-of-plane displacement $u_1(r,\theta)$ at the interface, for $\gamma = 1$, is shown in Fig. 4, where the number of shadow terms is increased up to $S_1 = 8$. It is observed that the solution is not so different between $S_1 = 4$ and $S_1 = 8$. Moreover, the constant main term, $S_1 = 0$, of the unit value can be observed along the Neumann and Robin boundary parts, since it is the solution to the Neumann–Neumann problem. The displacement value at the origin of polar coordinates is $u_1(0,0) = u_1(0,\pi) = 1$, which can be used to define the *Generalized Stress Intensity Factor* K_1, introduced in (17), as the half of the jump, across the interface, of the crack-tip value of the displacement in any antiplane-strain BVP including a crack on a spring interface. It is also interesting to observe that $u_1(r,\theta)$ decreases with growing r on the Robin interface.

The evolution of $u_1(r,\theta)$ when γ is changed is shown in Fig. 5 on the bottom boundary of the half-plane Ω^+ (at $\theta = 0$ and π) for $\gamma = 1$, $\gamma = 5$ and $\gamma = 10$. Both the number of shadow terms for each γ and the range of representation, $r \in (0 - 0.15)$, have been selected considering that the relative error in the Robin boundary condition should be similar in the three cases. This is explained at the end of this section. It can be observed that at $\theta = 0$, where the linear elastic springs distribution is located, the displacement decreases when the parameter γ increases, because the spring interface is stiffer. The opposite effect is produced at $\theta = \pi$, where $u_1(r,\theta)$ increases with growing γ. Note that, for all the values chosen for γ, $u_1(0,0) = u_1(0,\pi) = 1$.

Fig. 6 shows stresses in the rectangle $[-1,1]\times[0,1]$, for $S_1 = 8$. It is observed that there is a logarithmic singularity in the two stress components when $r \to 0$. These stresses have a different behaviour especially on the bottom half-plane boundary. The logarithmic singularity is observed in $\sigma_{rz1}(r,\theta)$, shown in Fig. 6(a), on both the Robin and Neumann boundary parts, $\theta = 0$ and π, respectively, for $r \to 0$. However, this singularity is not observed on these boundary parts in $\sigma_{\theta z1}(r,\theta)$, shown in Fig. 6(b), where it vanishes on the Neumann part and it is bounded on the Robin part.

In Fig. 7 the approximation of the stress component $\sigma_{\theta z1}(r,\theta)$ by the asymptotic series is plotted on the Robin boundary part ($\theta = 0$) and the Neumann boundary part ($\theta = \pi$) for increasing number of shadow terms. The Neumann boundary condition is fulfilled at $\theta = \pi$, since $\sigma_{\theta z1}(r,\pi) = 0$. Notice that at the crack tip a discontinuity appears, $\lim_{r\to 0^+}\sigma_{\theta z1}(r,0) = 2k u_1(r,0) = 2k$, due to the Robin boundary condition, in the present case $2k = 1$, whereas $\lim_{r\to 0^+}\sigma_{\theta z1}(r,\pi) = 0$, due to the Neumann boundary condition. It is also observed that, although there is a stress singularity in the neighbourhood of the crack tip, it is not observed when the

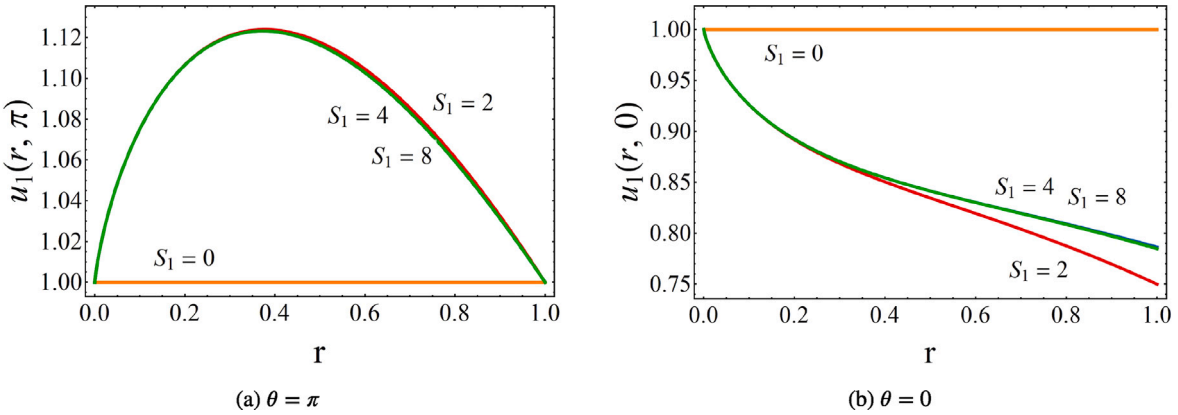

Fig. 4. Out-of-plane displacement $u_1(r, \theta)$ at the Neumann (a) and Robin (b) boundary parts, for several values of S_1 up to $S_1 = 8$, with $\gamma = 1$.

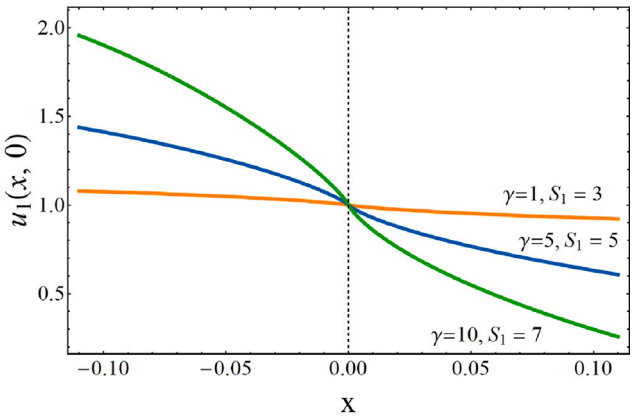

Fig. 5. Out-of-plane displacement $u_1(r, \theta)$ for several values of γ, at $\theta = 0$ and $\theta = \pi$.

solution is studied at the bottom boundary of the half-plane. For a better representation we have omitted the case of $S_1 = 0$, giving just the constant main term with $\sigma_{\theta z1}(r, \theta) = 0$, for all r and θ. Note that the curves for $S_1 = 2$ correspond to the expression in (49).

In Fig. 8(a) the stress component $\sigma_{rz1}(r, \theta)$ is represented on the Neumann boundary part, at $\theta = \pi$. Fig. 8(b) shows $\sigma_{rz1}(r, \theta)$ on the Robin boundary part, at $\theta = 0$. In this case a logarithmic singularity is observed in the vicinity of the crack tip. The curves for $S_1 = 2$ correspond to (50).

Finally, the relative error in the Robin boundary condition (36) is analysed. At first, Fig. 9 shows $e(r)$ for $0 \leq r \leq 1$, where it is observed that the accuracy of the solution increases near the crack tip with growing number of shadow terms S_1 included in the asymptotic series. Theoretically, if we had an infinite number of shadow terms, the solution would have zero error for all r. Nevertheless, the accuracy is strictly related to the computational complexity, thus, S_1 is limited in practice. The aim is to minimize S_1 for which $e_1(r) \ll 1$ for $0 \leq r \leq 1$. Attending to this balance between the accuracy and computational cost, $S_1 = 8$ is chosen for the 3D representations of the solution in Figs. 3 and 6, since the computational complexity is highly increased when $S_1 = 9$ is applied.

In the analysis presented in Fig. 5, the displacement behaviour for different values of γ was compared. In that figure, the number of shadow terms for each value of γ was selected to have a maximum relative error in the Robin boundary condition of 10^{-3}, for $0 \leq r \leq 0.11$. In Fig. 10 this error is represented for several values of γ, and the used number of shadow terms, S_1. As it could be expected, for higher values of γ more shadow terms are necessary to obtain the same accuracy in the solution.

7. Energy release rate calculated by the Irwin crack closure integral

To predict crack propagation along a spring interface, the calculation of the Energy Release Rate (ERR) G is fundamental. The issue of ERR for a crack in a spring interface has been analysed and discussed by several authors [11,13,14,21,34–39], in most cases apparently independently, which is somewhat surprising. Nevertheless, it is useful to compute G considering the present crack tip solution (17) by employing the Irwin crack closure integral [40].

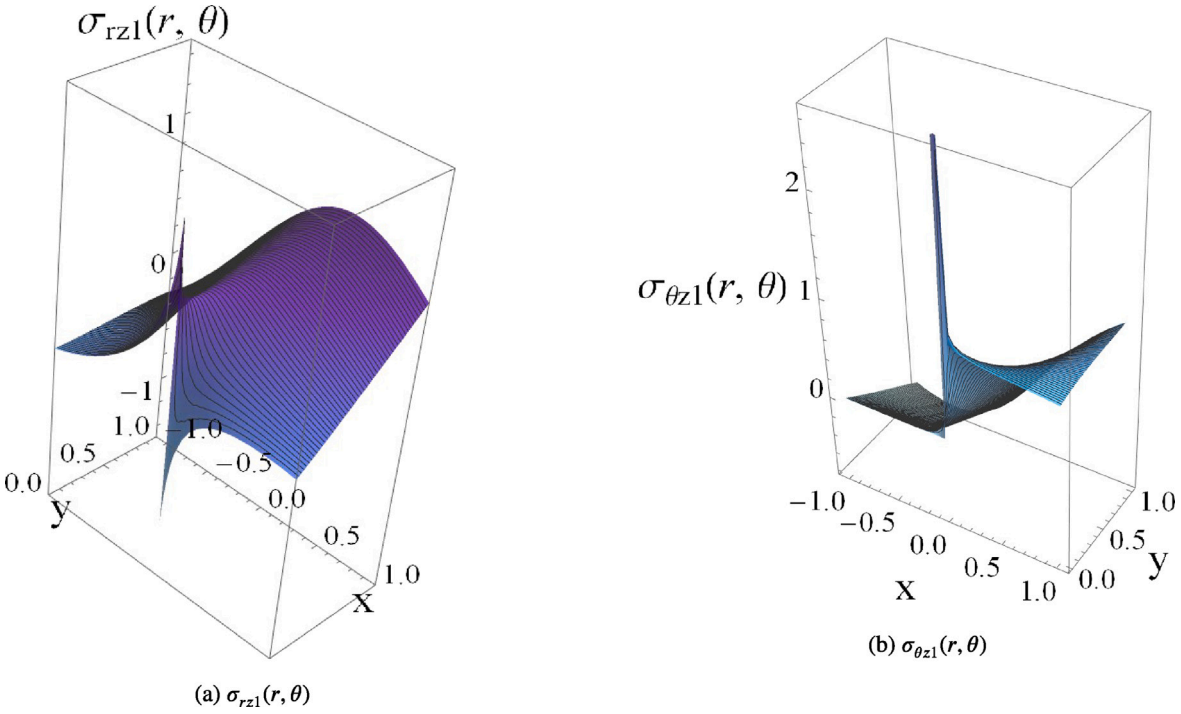

(a) $\sigma_{rz1}(r, \theta)$ (b) $\sigma_{\theta z1}(r, \theta)$

Fig. 6. Stress components in a rectangular plate, for $\gamma = 1$ and $S_1 = 8$.

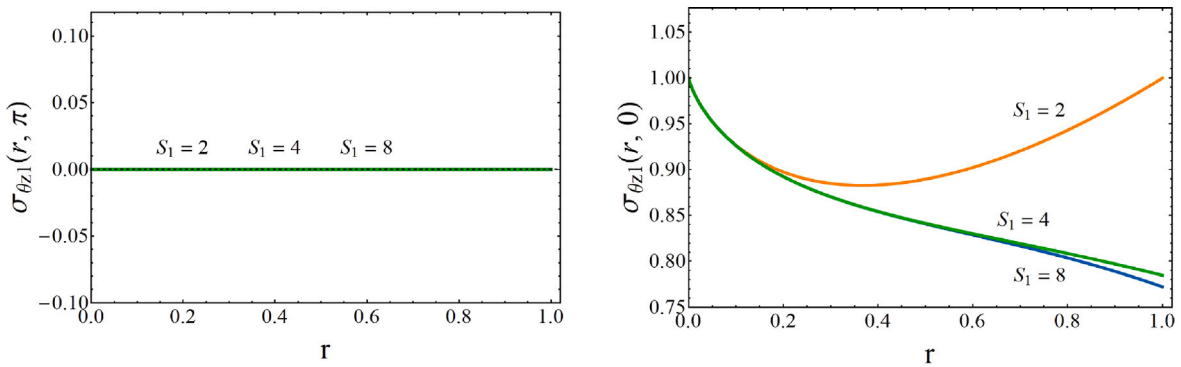

(a) $\theta = \pi$ (b) $\theta = 0$

Fig. 7. Stresses $\sigma_{\theta z1}(r, \theta)$ on the Neumann (a) and Robin (b) boundary parts, for $\gamma = 1$.

Considering the decomposition of the solution into the even and the odd part, see Section 2, and given that the interface shear traction and the relative displacement of the even part are zero on the interface, it is sufficient to consider only the odd part of the solution analysed in Sections 3–6.

As follows from the asymptotic series expansion (17) and the expressions of its terms in Section 5, the interface displacement u_z is continuous along the interface, having however an infinite derivative at the crack tip. The only nonzero contribution to the crack tip value of displacement is provided by the main term $u_1^{(0)}$ which represents the unit rigid body translation, whereas the other remaining main and shadow terms vanish at the crack tip. Thus, the relative displacement at the crack tip is $2K_1$, where K_1 is the GSIF. Recall that the dimension of K_1 is length, see Section 3.

According to the expressions of stresses in Section 5, the interface shear traction σ_{yz} is discontinuous at the crack tip, having a finite one-sided limit approaching the crack tip from the spring interface part, with an infinite tangential derivative therein. The only nonzero contribution to the crack tip value of this interface shear traction is given by the first shadow term, whereas all the main terms and other remaining shadow terms evaluated on the interface vanish at the crack tip. Thus, the interface shear traction

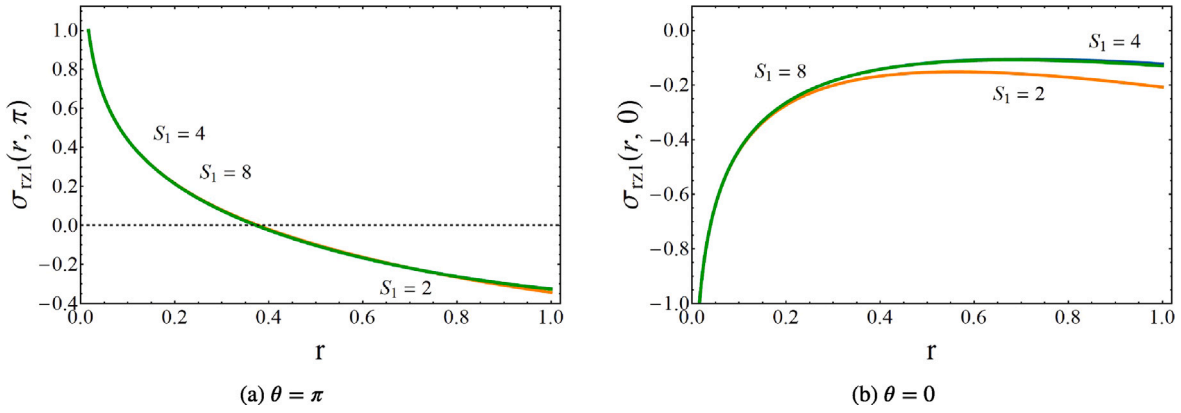

Fig. 8. Stresses $\sigma_{rz1}(r,\theta)$ on the Neumann (a) and Robin (b) boundary parts, for $\gamma = 1$.

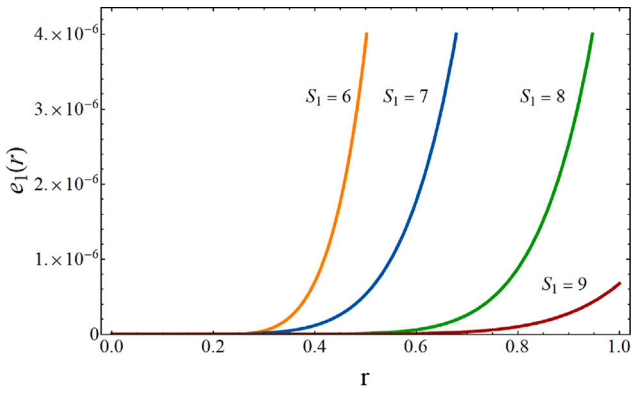

Fig. 9. Relative error in the Robin boundary condition $e_1(r)$ at $\theta = 0$, for several values of S_1, with $\gamma = 1$.

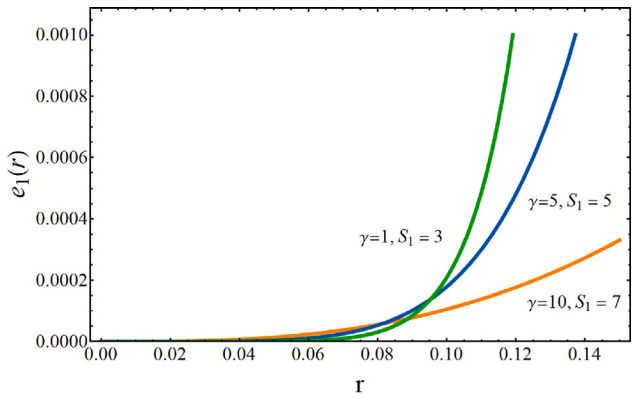

Fig. 10. Relative error in the Robin boundary condition $e_1(r)$ at $\theta = 0$, for several values of γ.

at the crack tip is $K_1\gamma\mu$. This value can also be computed by multiplying the relative displacement at the crack tip by the spring stiffness giving $k(2K_1)$.

Two elastic states for the interface crack are considered in the following analysis: the real state with the crack tip at the origin O of the Cartesian coordinate system as shown in Fig. 1, and the virtual δ-state with the crack length incremented by a small length $\delta > 0$, Fig. 11.

The Irwin crack closure integral involves the shear tractions in the real elastic state, $\sigma_{\theta z}(r,\theta = 0)$, and the relative displacement between crack faces in the virtual δ-state, $u_z^{\delta}(r,\pi) - u_z^{\delta}(r,-\pi) = 2u_z^{\delta}(r,\pi)$. Considering a unit thickness of the specimen, the limit of

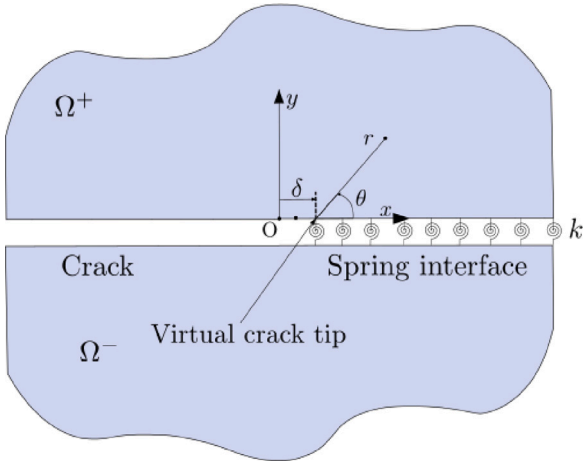

Fig. 11. Virtual crack in a straight spring (adhesive) interface with a small crack length increment $\delta > 0$ with respect to the real crack configuration.

the Irwin integral giving ERR G can be computed as

$$G = \lim_{\delta\to 0^+} \frac{1}{\delta}\int_0^\delta \frac{1}{2}\sigma_{\theta z}(r,0)\ 2u_z^\delta(\delta - r,\pi)\mathrm{d}r \overset{\text{mean theorem}}{=} \lim_{\delta\to 0^+} \frac{1}{2}\sigma_{\theta z}(r',0)\ 2u_z^\delta(\delta - r',\pi)$$
$$\overset{\substack{\text{continuity of displacement}\\ \text{variations from } \delta\text{-state to the real state}}}{=} \frac{1}{2}\sigma_{\theta z}(0,0)\ 2u_z(0,\pi) = \frac{1}{2}k(2K_1)^2 = 2kK_1^2, \tag{60}$$

where the first mean value theorem for integrals has been applied, with r' being a point in the virtual crack increment zone, i.e. $0 \le r' \le \delta$, and then the continuity of displacement variation between the δ-state and the real state for $\delta \to 0^+$ has been assumed, i.e. $\lim_{\delta\to 0^+} u_z^\delta(r,\pi) = u_z(r,\pi)$ at any point r on the interface, cf. [14,39]. The term $\frac{1}{2}\sigma_{\theta z}(0,0)\ 2u_z(0,\pi)$ represents the energy per unit area stored in the spring at the crack tip. Recall that $\sigma_{\theta z}(0,0)$ is given by the first shadow term, as the contribution of the main term to stresses is zero, and $u_z(0,\pi)$ is given by the main term, for $j = 1$.

8. Concluding remarks

In this paper, a new asymptotic linear elastic solution for semi-infinite cracks in a straight spring interface, modelled by a continuous spring distribution, has been deduced and analysed for antiplane strain state. The solution of this crack problem has been split into a regular even (symmetric) part and a singular odd (skew-symmetric) part with respect to a straight interface. While the regular solutions are given by linear combinations of a subset of homogeneous harmonic polynomials, the deduction of the singular solutions is much more sophisticated because their expressions include an infinite series of shadow terms associated with each smooth main term. For the first time, it has been shown that all these shadow terms include the powers of the logarithmic function increasing with the order of the shadow term. The corresponding Neumann–Robin and Robin–Neumann problems in the upper half-plane are analysed to describe the behaviour of the linear elastic singular solution in the vicinity of the crack tip in a spring interface.

The Neumann–Robin problem in the half plane, can be considered as a particular case of the Neumann–Robin problem for a corner given by an angular sector of angle ω studied in [30], considering $\omega = \pi$ in the present case of half-plane. However, the present procedure used to obtain the singular solution for the half-plane has been simplified and is more explicit with respect to that for a general corner. Following a technique inspired in the Gaussian back substitution, the unknown coefficients $b_{j,k}^{(0)}$ of the general expression proposed are explicitly calculated using more simplified expressions due to the fact that the boundary conditions are applied at $\theta = 0$ and π. This is very important from the point of view of the computational complexity, since the asymptotic series with more shadow terms can be easily computed, obtaining a lower error in the Robin boundary condition.

A clear enhancement in the accuracy of the approximate solution is observed for growing number of shadow terms S_j. This is specially important when the material properties plays a major role, i.e., when the ratio of the spring stiffness k and the shear modulus of the adherent material μ is increasing.

A successful numerical verification of the analytic solution deduced in the present work has been made in [41] by the FEM code FEniCS, and in [42] by the Matlab FEM code [43] modified to include the Robin boundary condition.

A logarithmic singularity is observed in the stress components, $\sigma_{\theta z}$ and σ_{rz} at the crack tip. However, due to the imposition of the homogeneous Neumann and Robin (spring) boundary conditions for the half-plane problem, this singularity is not observed in the tractions on the spring interface, where these tractions are bounded, just a discontinuity in the interface tractions and a singularity in the gradient (tangential derivative) of these tractions occur at the crack tip. In fact, this logarithmic singularity in the gradient of shear tractions and equivalently also in the gradient (tangential derivative) of displacements on the spring interface makes often

difficult to compute the crack tip values of shear tractions and displacements in this spring interface. Since, as it has been shown, these maximum values determine the Energy Release Rate (ERR) of the crack, an accurate calculation of these values is crucial in the prediction of crack growth along the spring interface.

To improve the accuracy of the calculation of these crack tip values, the obtained analytical approximation of the singular solution can be implemented in the shape functions of singular or enriched finite elements in the vicinity of the crack tip on spring-interface, for a better representation of the exact solution, reducing the computational complexity of such calculations. The first crack tip element with logarithmic singularity of stresses of this type has recently been implemented and successfully tested in [42].

In practical applications it can be useful to work with the following dimensionless governing parameter, instead of that defined in (15),

$$\gamma = \frac{2kL}{\mu}, \tag{61}$$

where L is a characteristic length in the studied problem, as the finite crack size or the thickness of the adherent layer in a laminate, etc. The corresponding dimensionless expressions of the main and shadow terms in the asymptotic series expansion (17) could be derived, however they are not presented here for the sake of simplicity of the expressions.

The asymptotic series expansion for a crack in a spring (Robin) interface deduced in the present work can be considered as the first step towards the derivation of the crack tip solution for widely used cohesive cracks with intrinsic cohesive laws.

Noteworthy, although the present work is focused on crack-tip solutions with non-negative singularity exponents $\lambda \geq 0$, i.e., with a finite strain energy in the vicinity of crack tip, we have checked that the present procedure can be adapted to compute crack-tip solutions with negative singularity exponents $\lambda < 0$, with an infinite strain energy in the vicinity of crack tip. These solutions with $\lambda < 0$, usually referred to as quasi-dual functions including the dual main terms and the associated dual shadow terms, might be used to extract GSIFs K_j in (17), in a similar way as in the Quasi-Dual Function Method (QDFM) developed in [20,44], for extraction of Edge SIFs (ESIFs) along a crack front in a 3D fracture problem.

In view of other physical interpretations of the Robin boundary condition as, e.g., thermal boundary resistance condition in heat transfer and impedance conditions in electro-magnetics and acoustic, this solution can be applied to solve analogous problems governed by the Laplace equation in other engineering branches.

CRediT authorship contribution statement

Sara Jiménez-Alfaro: Writing – review & editing, Writing – original draft, Visualization, Validation, Software, Methodology, Investigation. **Vladislav Mantič:** Writing – review & editing, Writing – original draft, Supervision, Methodology, Investigation, Conceptualization.

Declaration of competing interest

The authors declare that they have no known competing financial interests or personal relationships that could have appeared to influence the work reported in this paper.

Data availability

No data was used for the research described in the article

Acknowledgements

V.M. acknowledges that Dr. Alberto Salvadori (University of Brescia) inspired the present work by his preliminary research carried out during his brief research stay at the University of Seville in 2009. The present research was conducted with the support of Spanish Ministry of Science and Innovation: PID2021-123325OB-I00, Consejería de Económía, Conocimiento, Empresas y Universidad, Junta de Andalucía: P18-FR-1928; European Regional Development Fund: P18-FR-1928. The funding received from the European Union's Horizon 2020 research and innovation programme under Marie Sklodowska-Curie grant agreement No. 861061-NEWFRAC is gratefully acknowledged.

Appendix A. Supplementary data

Supplementary material related to this article can be found online at https://doi.org/10.1016/j.engfracmech.2023.109293.

References

[1] Winkler E. Die Lehre von der Elasticität und Festigkeit mit besondere Rücksicht auf ihre Anwendung in der Technik, für polytechnische Schulen, Bauakademien, Ingenieure, Maschienenbauer, Architecten, etc.. Prag: Verlag von H. Dominicus; 1867.
[2] Volkersen O. Die Nietkraftverteilung in Zugbeanspruchten Nietverbindungen mit Konstanten Laschen-querschnitten. Luftfahrtforschung 1938;15:41–7.
[3] Goland M, Reissner E. The stresses in cemented joints. J Appl Mech 1944;11:A17–27.
[4] Hart-Smith LJ. Analysis and design of advanced composite bonded joints. Technical report, NASA CR-2218, 1974.
[5] Dillard DA, Mukherjee B, Karnal P, Batra RC, Frechette J. A review of Winkler's foundation and its profound influence on adhesion and soft matter applications. Soft Matter 2018;14:3669–83.
[6] Benveniste Y, Miloh T. Imperfect soft and stiff interfaces in two-dimensional elasticity. Mech Mater 2001;33:309–23.
[7] Javili A, Kaessmair S, Steinmann P. General imperfect interfaces. Comput Methods Appl Mech Engrg 2014;275:76–97.
[8] Tserpes K, Barroso-Caro A, Carraro PA, Carrillo Beber V, Floros I, Gamon W, Kozłowski M, Santandrea F, Shahverdi M, Skejić D, Bedon C, Rajčić V. A review on failure theories and simulation models for adhesive joints. J Adhes 2022;98(12):1855–915.
[9] Prandtl L. Ein Gedankenmodell für den Zerreißvorgang spröder Körper (A thought model for the fracture of brittle solids). Z Phys Angenw Math Mech 1933;13(2):129–33, Translation: Knauss W. G., Int J Fract (2011) 171:105–109.
[10] Destuynder P, Michavila F, Santos A, Ousset Y. Some theoretical aspects in computational analysis of adhesive lap joints. Internat J Numer Methods Engrg 1992;35:1237–62.
[11] Erdogan F. Fracture mechanics of interfaces. In: Rossmanith HP, editor. Damage and failure of interfaces. Rotterdam: Balkema Publishers; 1997, p. 3–36.
[12] Geymonat G, Krasucki F, Lenci S. Mathematical analysis of a bonded joint with a soft thin adhesive. Math Mech Solids 1999;4:201–25.
[13] Lenci S. Analysis of a crack at a weak interface. Int J Fract 2001;108:275–90.
[14] Mantič V, Távara L, Blázquez A, Graciani E, París F. A linear elastic - brittle interface model: Application for the onset and propagation of a fibre-matrix interface crack under biaxial transverse loads. Int J Fract 2015;195:15–38.
[15] Kondratiev VA. Boundary-value problems for elliptic equations in domains with conical or angular points. Trans Moscow Math Soc 1967;16:227–313.
[16] Costabel M, Dauge M. Construction of corner singularities for Agmon-Douglis-Nirenberg elliptic systems. Math Nachr 1993;162(1):209–37.
[17] Wieghardt K. Über das Spalten und Zerreissen elastischer Körper (On splitting and cracking of elastic bodies). Z Math Phys 1907;55(1–2):60–103, Translation: Rossmanith H.P., Fatigue Fract Engng Mater Struct (1995) 12:1371–1405.
[18] Williams ML. On the stress distribution at the base of a stationary crack. J Appl Mech 1957;24(1):109–14.
[19] Paris PC, Sih GC. Stress analysis of cracks, Vol. 381. ASTM STP26584S, Philadelphia: ASTM; 1965, p. 30–81.
[20] Yosibash Z. Singularities in elliptic boundary value problems and elasticity and their connection with failure. New York: Springer; 2012.
[21] Destuynder P, Michavila F, Ousset Y, Santos A. Utilisation du taux de restitution de l'energie dans l'analyse a deux échelles de l'endommagement d'un joint collé. C R Acad Sci Paris 1990;310 Serie I:161–5.
[22] Sinclair GB. A note on the removal of further breakdowns in classical solutions of Laplace's equation on sectorial regions. J Elasticity 1999;56:247–52.
[23] Mishuris G. Interface crack and nonideal interface concept (Mode III). Int J Fract 2001;107:279–96.
[24] Mishuris GS, Kuhn G. Asymptotic behaviour of the elastic solution near the tip of a crack situated at a nonideal interface. ZAMM Z Angew Math Mech 2001;81(12):811–26.
[25] Antipov YA, Avila-Pozos O, Kolaczkowski ST, Movchan AB. Mathematical model of delamination cracks on imperfect interfaces. Int J Solids Struct 2001;38(36–37):6665–97.
[26] Sinclair GB. On the influence of cohesive stress-separation laws on elastic stress singularities. J Elasticity 1996;44:203–21.
[27] Sinclair GB. A note on the influence of cohesive stress-separation laws on elastic stress singularities in antiplane shear. J Elasticity 2009;94:87–93.
[28] Sinclair GB. On the influence of adhesive stress-separation laws on elastic stress singularities. J Elasticity 2015;118:187–206.
[29] Mghazli Z. Regularity of an elliptic problem with mixed Dirichlet-Robin boundary conditions in a polygonal domain. Calcolo 1992;29(3–4):241—267.
[30] Jiménez-Alfaro S, Villalba V, Mantič V. Singular elastic solutions in corners with spring boundary conditions under anti-plane shear. Int J Fract 2020;223:197–220.
[31] Wolfram S. Mathematica, A system for doing mathematics by computer. Redwood City: Addison-Wesley; 1991.
[32] Medková D. The Laplace equation: Boundary value problems on bounded and unbounded Lipschitz domains. Cham: Springer; 2018.
[33] Baranova S, Mogilevskaya SG, Mantič V, Jiménez-Alfaro S. Analysis of the antiplane problem with an embedded zero thickness layer described by the Gurtin-Murdoch model. J Elasticity 2020;140(2):171–95.
[34] Entov VM, Salganik RL. On the Prandtl brittle fracture model. Mech Solids 1968;3(6):79–89, (Translated from Russian).
[35] Fernlund G, Spelt JK. Analytical method for calculating adhesive joint fracture parameters. Eng Fract Mech 1991;40:119—132.
[36] Krenk S. Energy release rate of symmetric adhesive joints. Eng Fract Mech 1992;43(4):549–59.
[37] Bruno D, Greco F. Mixed mode delamination in plates: a refined approach. Int J Solids Struct 2001;38:9149–77.
[38] Shahin K, Taheri F. The strain energy release rates in adhesively bonded balanced and unbalanced specimens and lap joints. Int J Solids Struct 2008;45:6284—6300.
[39] Carpinteri A, Cornetti P, Pugno N. Edge debonding in FRP strengthened beams: Stress versus energy failure criteria. Eng Struct 2009;31:2436–47.
[40] Irwin GR. Analysis of stresses and strains near the end of a crack traversing a plate. J Appl Mech 1957;24:361–4.
[41] Jiménez-Alfaro S, Mantič V. FEM benchmark problems for cracks with spring boundary conditions under antiplane shear loadings. Aerotec Missili Spaz 2020;99(4):309–19.
[42] Mantič V, Vázquez-Sánchez A, Romero-Laborda M, Muñoz-Reja M, Jiménez-Alfaro S, Távara L. New crack-tip element for the logarithmic stress-singularity of cracks on spring interfaces in mode III, Comput Methods Appl Mech Eng (to be submitted).
[43] Alberty J, Carstensen C, Funken SA. Remarks around 50 lines of matlab: short finite element implementation. Numer Algorithms 1999;20(2):117–37.
[44] Yosibash Z, Schapira Y. Edge stress intensity functions along elliptic and part-elliptic 3D cracks. Eng Fract Mech 2021;245:107477.